Title

Strength of the geomagnetic field in the Cretaceous Normal Superchron: New data from submarine basaltic glass of the Troodos Ophiolite

Journal

Geochemistry Geophysics Geosystems, 5

ISSN

1525-2027

Authors

Tauxe, Lisa
Staudigel, H

Publication Date

2004-02-01

Peer reviewed

Strength of the Geomagnetic Field in the Cretaceous Normal Superchron: New Data from Submarine Basaltic Glass of the Troodos Ophiolite

Lisa Tauxe

Geosciences Research Division,Scripps Institution of Oceanography, La Jolla, CA 92093-0220, USA

Hubert Staudigel

Institute for Geophysics and Planetary Physics, Scripps Institution of Oceanography, La Jolla, CA 92093-0225, USA

Abstract.
We present here new paleointensity data from 39 sampling sites collected from the quenched margins of pillow lavas and dikes exposed within the Troodos Ophiolite ($\sim$ 92 Ma), formed during the Cretaceous Normal Superchron (CNS), a period of approximately 40 million years when the geomagnetic field reversed extremely infrequently if at all. Monte Carlo simulations suggest that a minimum of 25 estimates are necessary for a reasonably robust estimate for the average field strength. Our data suggest a dipole strength equivalent to the present field or nearly twice the post-CNS average. The mean and standard deviation of the dipole moment (81 ± 43 ZAm^2) from the 57 data points compiled here agree remarkably well those predicted from the long paleointensity record derived from DSDP Site 522. The new data set for the CNS suggests a picture of a strong and stable field during the period of time when it stopped reversing. Moreover, the similarity of the CNS data with the present geomagnetic field suggests that it is presently in a state of unusual polarity stability.

1. Introduction

After decades of effort, much is known about the behavior of the geomagnetic field. The present dipole moment is about 80 ZAm^2. ["Z" stands for Zetta (10^{21})]. We know that the frequency of reversals has changed profoundly through time from periods of frequent reversals (as for the last 50 million years) to periods of no reversals for some 40 or more million years (as in the mid-Cretaceous and the Permian). We know that when the field reverses, its strength drops to extremely low values (e.g., *Prévot et al.* [1985]). We do not know what causes reversals or what inhibits them, although numerical simulations have provided some tantalizing hints (e.g., *Glatzmaier et al.* [1999]). The observation that reversals are associated with low field strength suggests the possibility that low fields are a precondition for reversal and that a high average field strength would inhibit the reversal process (e.g., *Larson and Olson* [1991], but see also *Loper and McCartney* [1986]). Furthermore, the precipitous drop in field strength over historic times has led some to the speculation that the field is headed toward a reversal (e.g., *Hulot et al.* [2002]). Yet, if the field is at a relatively high value compared to average (e.g., *Juarez and Tauxe* [2000]), a reversal could be less likely. The strength of the field during periods of no reversals is therefore of general interest. The data, however, are scarce.

There have been many compilations of paleointensity data over the last decade based on the so-called PINT database initiated by *Tanaka et al.* [1995] and currently maintained by *Perrin et al.* [1998]. The most recent version is available at:
ftp://ftp.dstu.univ-montp2.fr/pub/paleointdb/2002/).

We have modified the PINT database in two ways. We have added the data included in: *Goguitchaichvili et al.* [2002c, a, b, 2003]; *Riisager et al.* [2001]; *Shi et al.* [2002]; *Tanaka and Kono* [2002]; *Tarduno et al.* [2001, 2002]; *Selkin and Tauxe* [2000], and, each of the paleofield estimates were converted to virtual axial dipole moments (VADMs) using paleolatitudes derived from a self consistent set of rotations derived from *Besse and Courtillot* [2002]. Most compilations quote dipole moments in terms of virtual dipole moment (VDM) which do not rely on reconstructed paleolatitudes, but use instead a mean inclination value to estimate magnetic paleolatitude. The quality of the mean inclinations are highly variable and in many cases (when using unoriented material) are not available at all. We prefer the more robust and self consistent practice of using a model for global plate reconstruction to estimate paleolatitude and then calculate a VADM. The differences between VDM and VADM are usually minor however.

From the database thus constructed we have selected data from 1-160 Ma that were obtained from Thellier-Thellier experiments (with pTRM checks; see *Coe et al.* [1978]). We excluded explicitly transitional data and data for sites with only one specimen. There are two ways of rejecting site means based on their within site scatter. One is to set a value in terms of absolute field (e.g., $\leq$ 5 mT). The other is to set a value for the percent deviation ($100\sigma/\bar{B}$), say 15%. The former is difficult to achieve for high mean values and the latter biasses against low values. We therefore require sites to meet one or the other for inclusion in our compilation. The updated dataset (including several corrections of typos) is available in the MagIC database (http://earthref.org).

There are six studies in this compilation with data from the Cretaceous Normal Superchron (CNS; *Riisager et al.* [2001]; *Tanaka and Kono* [2002]; *Juarez et al.* [1998]; *Cottrell and Tarduno* [2000]; *Tarduno et al.* [2001, 2002]). These studies have from one to five sites meeting our minimum reliability criteria for a total of 18 data points. Taken together, the average of these data is 95 $\pm$ 44 ZAm^2, or significantly higher than the present dipole moment.

The question arises as to how many data points are required to robustly estimate paleofield strength. We address this with a Monte Carlo simulation, by taking random samples of a statistical geomagnetic field model of the type described by *Constable and Parker* [1988]. We choose the TK03.GAD model of *Tauxe and Kent* [in press] for this simulation. We randomly draw N values of intensity, convert them to VADMs and calculate the mean and standard deviation as a function of N. A typical run is shown in Figure 1. From this simple simulation, it is evident that at least 25 paleofield estimates are required and that 18 might result in an biased result. Certainly, none of the individual studies has temporal sampling sufficient to provide a robust estimate of the paleofield during the CNS.

The dearth of paleointensity data for the CNS stems from the difficulty of finding material suitable for the most reliable method of paleointensity determination, the Thellier-Thellier experiment. The Thellier-Thellier experiment requires material whose magnetic phase is small enough to lack domain walls, yet large enough to retain a stable magnetization. Differences in cooling rate during acquisition of thermal remanence between the original and laboratory cooling strongly effects the ancient field estimate, so the ancient cooling rate must be reasonably well known, and if different from the laboratory cooling rate, the estimated field must be corrected (e.g., *Selkin et al.* [2000]). Furthermore, as the experiment entails repeated heating to progressively higher temperatures, the magnetic phase may not change its capacity to acquire a thermal remanence during the experiment. Submarine basaltic glass (SBG), formed when basalt is extruded into seawater and chills rapidly often is such a material (e.g., *Pick and Tauxe* [1993a, b, 1994]).

SBG is by nature highly susceptible to weathering. It can alter to hydrous phases and disappear from the geological record. Yet, ancient SBG can be found both in drill cores (e.g. from the Ocean Drilling Program (e.g., *Selkin and Tauxe* [2000]) and in outcrop (e.g., *Robinson et al.* [1983]). In this paper we exploit the fact that the Troodos Ophiolite formed during the CNS at about 92 Ma (*Mukasa and Ludden* [1987]) and has been exhumed, exposing remarkable outcrops of the ancient seafloor extrusives, including abundant submarine basaltic glass (*Robinson et al.* [1983]; *Rautenschlein et al.* [1985]).

1.1. The origin of remanence in SBG

The use of SBG for paleointensity measurements relies on a high temperature origin of its remanence. *Heller et al.* [2002] challenged this, arguing that low Ti magnetite is not an equilibrium phase in MORB (citing *Buddington and Lindsley* [1964]) and therefore it must be of low temperature origin. They propose that the primary high temperature Fe phase is Ti magnetite and speculate that the remanence in SBG is carried by low Ti magnetite that exsolves from high Ti magnetite after the glass has cooled down to 2°C. While clearly

expressing that no such a process is presently known, *Heller et al.* [2002] further speculate that SBG "probably contains a grain-growth chemical remanent magnetization in magnetite". While *Heller et al.* [2002] fail to offer supporting evidence for their proposed low temperature origin of SBG magnetization, there is a growing body of evidence that supports the high temperature origin.

We know that the magnetite in the SBG forms very quickly as demonstrated by its presence in fresh material retrieved within a year of eruption. Glass samples from three separate flows whose eruption ages are very well known have been analyzed for paleointensity studies. *Pick and Tauxe* [1993b] analyzed samples from the so-called "BBQ" site (9°N on the East Pacific rise) erupted in 1990 which was sampled about a year later. *Carlut and Kent* [2000] analyzed samples from two flows from the Juan de Fuca ridge whose eruptions were detected using sonic and seismic methods. The first (the "New Flow") erupted in 1993 and was sampled within a month (*Embley et al.* [1995]. The second erupted in January, 1998 and was sampled in July-September 1998 (*Embley et al.* [1999]). Fine grained basalts from the New Flow were analyzed by *Kent and Gee* [1996]. *Carlut and Kent* [2000] also analyzed samples from the so-called "Animal Farm" Site on the Southeast Pacific Rise, but the eruption age is imprecisely known. All of these samples had magnetic properties typical of SBG, with blocking temperatures between 430 and 574°C, indicating low-titanium magnetite as the carrier of remanence. More importantly, the flows that had highly reproducible results (a requirement for a successful paleointensity experiment) yielded "paleofield" estimates in excellent agreement with the known field at the time of eruption.

A second line of argument is based on kinetics. Magnetite begins demonstrably to grow when the samples are heated to above $\sim 600°$ C (Curie temperature experiments of *Pick and Tauxe* [1994]), but does not seem to do so at ambient temperatures. The magnetizations since the samples were first acquired do not change significantly during storage - in other words, magnetite is not currently growing in the samples. Furthermore, grain growth CRM theoretically is about 0.4 of a TRM acquired in the same field (*Stacey and Banerjee* [1974]). Therefore, it seems hardly credible that magnetite would exsolve at 2°C within one month of eruption and acquire a grain-growth CRM that yields present field values from a paleointensity experiment.

There is abundant petrologic evidence to suggest that low titanium magnetite forms as a high temperature phase in submarine basaltic glass (e.g., *Zhou et al.* [1997, 1999b, a]; *Xu et al.* [1997b, a]). For example, *Zhou et al.* [1997] studied basalts from the New Flow and found that while the large opaque oxides had the expected titanomagnetite composition (TM60), the interstitial glass had submicron titanomagntite grains with a broad range of titanium substitution ($0 < x < 0.8$). The discrepancy between the titanium substitution expected from equilibrium crystallization (cited by, for example, *Heller et al.* [2002]) and that actually observed in interstital and rim glasses of freshly made glass can be reconciled by recognizing the fact that glass is not an equilibrium phase and arguments based on phase equilibria do not apply.

The evidence therefore suggests overwhelmingly that low Ti magnetite in SBG can form as a high temperature phase, that it can evade alteration for geologically significant periods of time and that it can retain a primary thermal remanence yielding excellent paleointensity results. *Juarez et al.* [1998] published preliminary data from 5 specimens from SBG obtained from the Troodos Ophiolite, suggesting that the material behaves well during the Thellier-Thellier experiment. Based on these arguments, we undertook an extensive sampling and laboratory program to exploit the CNS aged SBG exposed in the Troodos Ophiolite.

2. Sampling and laboratory analysis

In April, 2002, we sampled submarine basaltic glass (SBG) from 76 sites in four regions of the Troodos Ophiolite (see Figure 2). Glass was taken from the margins of sheet flows and intact pillows, dikes, and sills and from pillow margin breccias and glassy flows (hyaloclastites) (see Figure 3).

Samples were first physically disaggregated with a mortor and pestle. This procedure is necessary to remove altered zones, but precludes the preservation of orientation. Individual pieces of glass up to 1 cm in width were washed in dilute HCl and examined under a binoculor microscope. Specimens that were free from signs of alteration, were unscratchable by a nonmagnetic steel blade, and had net magnetic moments in excess of 1 nAm^2 were placed in clean glass vials and fixed into position with microfiber glass filter papers. Thermal remanences of empty glass vials after heating to 600°C and cooling in a laboratory field (25 μT) were less than 10 pAm^2.

A total of 356 Troodos glass specimens were subjected to Thellier-Thellier type experiments (*Thellier and Thellier* [1959]). 293 were treated as follows. Glass

specimens were heated to 100°C and cooled in zero field. After measuring the natural remanent magnetization (NRM), the specimens were re-heated to 100°C, cooled in a laboratory field of either 25 μT or 40 μT, directed along the specimen's "Z" axis and remeasured. The difference in the z component between the second step and the first is the partial thermal remanence (pTRM) gained by cooling from 100°C to room temperature. This zero-field, in-field (or ZI) heating procedure was repeated at 50 degree intervals up to 200 degrees and then at 25 degree intervals with the addition of an extra step between the zero field and the in-field steps: a reheating to a lower temperature step and cooling in the laboratory field. The pTRM gained in this repeated step (the so-called pTRM check of, for example, *Coe et al.* [1978]), is compared with the first in field step at the same temperature. A difference is an indication of a change in the capacity of the specimen to acquire pTRM.

The remaining 63 specimens were subjected to a slightly different experimental procedure referred to here as the IZZI protocol. At every other temperature step, the order of the double heating procedure (zero-field, in-field, ZI) is reversed such that specimens are cooled in-field first, then in zero field (IZ). Also, after the ZI steps, the specimens are heated for a third time to the same temperature and cooled in zero-field. This so-called pTRM tail check step (e.g., *Riisager and Riisager* [2001]) is used to test if the pTRM gained when cooling in the lab field is entirely removed by reheating to the same temperature step, a necessary condition for reliable paleointensity determinations.

All specimens that were subjected to the IZZI experiment were removed from the glass tubes and measured on a Princeton Measurements Corp. Micromag alternating gradient force magnetometer for magnetic hysteresis. All measurements were made at room temperature. In addition, at least two uncooked "sister" specimens from the same sites were also measured.

3. Results

3.1. Thellier-Thellier experiments

The quality of the data from the Thellier-Thellier experiments can be assessed in a number of ways. Every paleointensity study encounters different behavior and must be judged in context. There are many parameters in the literature that describe behavior during the Thellier experiment some of which we find useful here.

Consider the data depicted in Figure 4. The points selected for the calculation of the best-fit slope ($|b|$) are solid circles and those omitted are open circles. The ancient field esitmate B_{anc} is the absolute value of this slope times the laboratory field. The "scatter parameter" β is the standard error of the slope over $|b|$ (e.g., *Coe et al.* [1978]). *Coe et al.* [1978] also advocated the use of the parameter f which is the fraction of the NRM component used in the slope estimation. This is found by extending the best fit line through the chosen component as shown by the heavy dashed line in Figure 4. The parameter f is the ratio of the NRM fraction (vertical dashed line) and the component of the NRM (circled intersection). We find that while f works well with single component magnetizations, it is misleading when there are multiple components of remanence as in, for example Figure 4. The value of f for this specimen is quite high, whereas the fraction of the total NRM is much less. We prefer to use a parameter f_{vds} which is the fraction of the total NRM, estimated by the vector difference sum (VDS) of the entire zero field demagnetization data (see Figure 4). The VDS "straightens out" the various components of the NRM by summing up the vector differences at each demagnetization step.

The difference between the original pTRM at a given temperature step (horizontal component of the circles in Figure 4) and the pTRM check (horizontal component of the triangles in Figure 4), δ_i (see Figure 4), can result from experimental noise or from alteration during the experiment. *Selkin and Tauxe* [2000] normalized the maximum δ_i value within the region of interest by the length of the hypotenuse of the NRM/pTRM data used in the slope calculation (the solid line through the selected data points). Their DRAT parameter is therefore the maximum Difference RATio. In many cases it is useful to consider the trend of the pTRM checks as well as their maximum deviation. We find therefore the sum of the differences more useful than the maximum δ_i. Here, we normalize this difference sum by the pTRM acquired by cooling from the maximum temperature step used in the slope calculation to room temperature. This parameter, expressed as a percentage, is called the Difference RATion Sum or DRATS.

The pTRM tail check step is a rather new addtion to the Thellier experimental protocol family. The absolute value of the difference between the original NRM measured at a given temperature step (vertical component of the circles in Figure 4 and the second zero field step (known as the pTRM tail check) results from some of the pTRM imparted in the laboratory at T_i having unblocking temperatures that are different from T_i. The absolute value of these differences (Δ_i) are plotted as squares in Figure 4. The Maximum Difference, nor-

malized by the VDS of the NRM and expressed as a percentage is the parameter MD.

In addition to parameters derived from the NRM-pTRM data, *Pick and Tauxe* [1993a] used two additional parameters associated with the directional variation of the NRM (see insert of Figure 4). These are the Maximum Angle of Deviation (MAD) of *Kirschvink* [1980] of the selected component and the angle that that component makes with the origin. The latter we call the Deviation ANGle (DANG). MAD is a measure of the scatter in NRM directions and DANG tests whether the component selected is actually trending toward the origin.

In certain specimens, the IZZI protocol leads to rather interesting behavior, described in detail by *Yu et al.* [in review]. The data with pTRM checks (associated with triangles) are the zerofield-infield (ZI) steps (lighter circles) and the intervening steps are the infield-zerofield (IZ) steps (darker circles). Alternating the two results in a "zigzag" in some specimens (barely discernible in Figure 4).

We illustrate the use of our Thellier parameters and the IZZI protocol in Figure 5. The data shown in Figure 5a are typical of our best data. While many specimens behave like tg041j, 187 (52%) are problematic in at least one fundamental way.

In Figure 5b we plot data showing a dramatic drift in pTRM checks at increasing temperatures. This is accompanied by a downward trend in the NRM directions (toward the lab field direction), caused by alteration of the specimen during laboratory heating. One danger with data like these is that there is a strong tendency to chose data from the low temperature portion of the NRM. Because these samples are Cretaceous in age, there is a likelihood that they have been contaminated with a VRM. For this reason, we use only components with maximum blocking temperatures of at least 350°.

Two examples of zig-zagging during the IZZI experiment are shown in Figures 5c and d. The zig-zagging is strongly dependent on the direction of the NRM with respect to the laboratory field and is least evident when the NRM is perpendicular to the laboratory field (see Figure 5d which shows a strong zigzagging for tempertaure steps up to about 300° while the NRM is vertical down (see inset) and no zigzagging when the field is more horizontal. Because of this directional dependence, it is hard to quantify the zigzagging effect itself. We note however that in general, specimens that display zig-zagging have MD values of 4% or greater; these are excluded from further consideration here.

In order to choose appropriate cut-off values for the rest of the parameters described above, we take a new approach. We plot the cumulative distributions of the various quality parameters in Figure 6. The cumulative distribution functions (CDFs) for these parameters tend to exhibit an inflection point shown as the solid line. We use these inflection points as the criterion for acceptance as a convenient and reasonable way to identify the best data in this study. Based on these plots, we chose the following cut-offs for use in our paleointensity studies: DRATS ≤ 25; $\beta \leq .15$; $f_{vds} \geq .25$; DANG ≤ 15; MAD ≤ 15. Furthermore, we require that there be at least two pTRM checks with blocking temperatures below the maximum blocking temperature chosen. Specimens passing all selection criteria are of grade "A". Failure of any single criterion results in a grade of "B", failure of two, a grade of "C" and so on. Of the specimens measured for this study, 178 were grade "A". The rest have been eliminated from further consideration.

All measurement data and their interpretations are available in the MagIC data base at:

http://earthref.org.

By making all our data available, investigators with different preferences for selection criteria can re-analyze our data.

3.2. Hysteresis measurements

We summarize the hysteresis experiments in Figure 7. Representative loops are shown in the insets. The ratio of saturation remanence to saturation magnetization (M_r/M_s) is plotted against the coercive field (B_c) in the larger plot. These data range from highly coercive with high remanence ratios (e.g., tg001x, tg051i) to low coercive fields and remanence ratios (e.g., tg002i).

Many of the loops are wasp-waisted (e.g., tg040j, tg001x) suggesting a mixture of single domain and super-paramagnetic grains (e.g., *Tauxe et al.* [1996]). The Thellier-Thellier data for specimens with wasp-waisted loops (see tg040j in Figure 5a) are generally of very high quality.

Some loops (e.g., tg002i) are reminiscent of those produced by ensembles of magnetic grains whose remanence state is "vortex". Specimens with these vortex type loops appear to exhibit the most pronounced zigzag effect (see Figure 5d).

Smirnov and Tarduno [2003] suggested that hysteresis measurements could be used to detect alteration of specimens during the Thellier-Thellier experiment. They also suggested that old submarine basaltic glass may suffer from undetected alteration. Specimens that

altered significantly during our Thellier-Thellier experiment are circled in Figure 7. Unheated sister specimens are shown as plus signs. There does not appear to be a simple way to identify altered specimens from unaltered specimens on the basis of the hysteresis loops. Moreover, there is tremendous variety from multiple specimens from the same site so relying on "sister" specimens is risky.

We argue that because hysteresis loops can never be performed on the same specimens as those used for Thellier-Thellier experiments until the experiment has finished and that because there is a tremendous variety of behavior from specimen to specimen that the hysteresis loops cannot be used to judge a particular experimental result. Moreover, the pTRM check procedure is designed to test specifically for alteration and, particularly when used in conjunction with the IZZI protocol, there is little chance that significant changes in the capacity for a specimen to carry a pTRM will go undetected.

3.3. Average paleo field from the Troodos glasses

We calculate site means $\bar{B}$ for all sites with at least two estimates of paleointensity with a grade of "A" (Table 1). We have 39 sites meeting with σs of less than 5μT or 15%. The grand mean of these 33.6 $\pm$ 18.3 (1 σ) μT. If we assume a paleolatitude of the Troodos Ophiolite of 20° (see *Juarez et al.* [1998]), we calculate a Virtual Axial Dipole Moment (VADM) of 75 $\pm$ 41 ZAm^2.

3.4. Temporal sampling of the Troodos data set

We have obtained data from 76 sites, 39 of which meet optimal selection criteria. These come from Akaki Canyon and the Kampia mine region. The Akaki sites sample the lithologic units B-L of *Rautenschlein et al.* [1985] and span nearly the entire extrusive thickness, including 11 cycles of volcanic activity, separated by 100s to 1000s of years). The rest of the successful sites are from the Kampia Mine region some 10 km to the East (see Figure 2). These also span the entire crustal thickness (excluding the top $\sim$50 m which everywhere are too oxidized). Depending on the assumed spreading rate (2-5 cm/yr), the two regions are likely to be different in age by 0.2 to 0.5 million years. We therefore estimate that our successful sites represent a temporal sampling of at least a few hundred thousand years of geomagnetic field variability.

3.5. Comparison with other data sets

We plot the updated compilation of paleointensity data in Figure 8 as triangles and our new data as circles. In an earlier compilation, *Selkin and Tauxe* [2000] could find no significant difference between the period of low reversal frequency including the CNS and the early Cenozoic and the period of more rapid reversal frequency in the later Cenozoic. They noted however that there were very few data from the CNS itself.

Since the compilation of *Selkin and Tauxe* [2000], there have been several new studies which we have included in Figure 8 for a total of 18 paleofield estimates. As noted in the introduction and illustrated in Figure 1, this is perhaps too few for a robust estimate of the paleofield and its standard deviation. In this study, we have more than doubled the number of data points in the CNS for a total of 57. It may now be possible to make a meaningful statistical comparison between the CNS and the post-CNS data. We show cumulative distributions of these two data sets in Figure 9. The grand mean of the 57 CNS sites in the compilation is 81 $\pm$ 43 ZAm^2 or approximately equal to the present dipole field. This is significantly higher than the mean of the 180 post-CNS sites of of 56 $\pm$ 30 ZAm^2.

The result that the average VADM for the CNS is approximately equivalent to the present field resolves an apparent paradox. Long sedimentary paleointensity records suggested that the average strength of the field is related to the length of the polarity interval (*Tauxe and Hartl* [1997]; *Constable et al.* [1998]). The absolute paleointensity database rarely has sufficient data within a single polarity interval (with the exception of the Brunhes) to make the comparison between polarity interval length and average paleofield and *Selkin and Tauxe* [2000] could establish no such relationship. The sedimentary record of DSDP Site 522 (*Tauxe and Hartl* [1997]; *Constable et al.* [1998] is currently the only published data set with sufficient numbers of paleofield estimates and variation in polarity interval length with which to test the relationship between polarity interval length and average field strength. It is therefore interesting to compare the data from Site 522 and the compilation of data from the CNS presented here.

The relative paleointensity behavior for the 11 million year period of the Oligocene was published by *Tauxe and Hartl* [1997] (see also *Constable et al.* [1998]). We convert the relative paleointensity estimates to quasi-absolute estimates of the geomagnetic field in μT using the technique of *Constable and Tauxe* [1996] whereby average transitional field estimates are as-

sumed to be 7.5 μT. In Figure 10 we show the VGP latitudes versus the relative paleointensity. The mean of the transitional data points (as identified in the magnetostratigraphy) is shown as a square. Normalizing this value to 7.5 μT and assuming a paleolatitude of 32°S for DSDP Site 522 in the Oligocene results in estimated VADMs for the DSDP 522 magnetic stratigraphy. In Figure 11a we plot the average VADMs versus polarity interval length and in Figure 11b we plot the same versus the standard deviation of the data. Also shown are the mean and standard deviation of the CNS data compiled here (stars). The predicted mean VADM for the CNS (∼40 million years long) agrees remarkably well with that observed.

The results shown in Figure 11 suggest that when sufficient samples are available and when the paleointensity data are placed reliably within a Chron of known length, there is a relationship between polarity interval and paleofield strength. This observation supports the idea that strong fields inhibit reversals (*Cox* [1968]). Furthermore, as noted by *Constable et al.* [1998] that the standard deviation of paleofield estimates is proportional to the average field is also supported by the CNS data.

The average field during the CNS (when the field did not reverse) was the same as the present field. The average field for the post-CNS period (excluding the most recent field state of the last 1 million years) is much less. This observation would suggest that we are not heading for a reversal, but rather that the present field is unusually strong and perhaps is returning to the average, weaker state.

4. Conclusions

1. The published literature contains 18 data points from within the CNS that meet minimum reliability criteria. Monte Carlo simulations from a statistical field model suggest that a minimum of 25 data points are necessary to obtain a robust estimate for mean and standard deviation of the paleofield strength.

2. In this paper, we exploited the abundance of fresh submarine basaltic glass exposed in canyons dissecting the Troodos Ophiolite. Samples from 76 sites distributed all around the ophiolite were subjected to the traditional Thellier-Thellier experiment (e.g., *Coe et al.* [1978]) or the new so-called IZZI experimental protocol, whereby temperature steps cooling in a laboratory field first, then cooling in zero field (IZ) alternate with zero field first, then in-field (ZI) steps. Data from IZZI experiments are useful for detecting subtle pTRM tails that are not demagnetized by the same temperature in which they were acquired resulting in a distinctive "zig-zagging" in the NRM-pTRM plots.

3. We chose critical cut-off values for various selection parameters by using cumulative distributions, an arguably less biassed method of setting selection criteria than the arbitrary way it is usually done. Of the 356 specimens analyzed here, 169 met these criteria. A total of 39 sites had at least two specimens with a standard deviation of $\leq$ 5 mT or 15%. The sites span at least several hundred thousand years and the average paleofield estimate is 33.6 ± 18.3 μT. Assuming a paleolatitude of 20° yields a mean dipole of 75 ZAm^2, or approximately equal to the present dipole field.

4. The data presented here more than double the data meeting minimum criteria: obtained from Thellier-Thellier experiments (with pTRM checks), at least two specimens per cooling unit with standard deviations of either 5 μT or 15%. Combining the data presented here with the published data results in a grand mean for the Cretaceous Normal Superchron of 81 ± 43 ZAm^2 (N = 57), which is significantly larger than the mean of the post CNS data (84-1 Ma) of 55 ± 30 ZAm^2 (N = 180).

5. We converted the relative paleointensity estimates for the Oligocene magnetostratigraphic record of *Tauxe and Hartl* [1997] to VADMs using the method of *Constable and Tauxe* [1996]. These data were then averaged by polarity interval. The plots of mean VADM versus polarity interval length and standard deviation predict values for the CNS in reasonable agreement with those presented here.

6. The CNS appears to have been a period with an average dipole moment approximately equal to the present field. This observation suggests that perhaps the geomagnetic field is not racing toward transition as proposed by *Hulot et al.* [2002]. Rather it could well be simply returning to a more average field state.

Acknowledgements

We would like to acknowledge the cheerful field assistance of Daniel and Philip Staudigel. We thank Peter Selkin, Jeff Gee, Cathy Constable and Robert Parker for stimulating conversations. We especially wish to

thank Agnés Genevey who co-developed the IZZI protocol used here. We are grateful to Jason Steindorf who made all the measurements. The manuscript was improved through the reviews of Scott Bogue, Mike McElhinny and Dennis Kent whose help we gratefully acknowledge. This work was supported in part by NSF Grant No. 0003395 to LT.

References

Besse, J., and V. Courtillot, Apparent and true polar wander and the geometry of the geomagnetic field over the last 200 Myr, *J. Geophys. Res*, *107*, doi:10.1029/2000JB000,050, 2002.

Buddington, A., and D. Lindsley, Iron-titanium oxide minerals and synthetic equivalents, *Petrology*, *5*, 310–357, 1964.

Carlut, J., and D. Kent, Paleointensity record in zero-age submarine basalt glass: Testing a new dating technique for recent MORBs, *Earth Planet. Sci. Lett.*, *183*, 389–401, 2000.

Coe, R. S., S. Grommé, and E. A. Mankinen, Geomagnetic paleointensities from radiocarbon-dated lava flows on Hawaii and the question of the Pacific nondipole low, *J. Geophys. Res.*, *83*, 1740–1756, 1978.

Constable, C., and R. L. Parker, Statistics of the geomagnetic srecular variation for the past 5 m.y., *J. Geophys. Res.*, *93*, 11,569–11,581, 1988.

Constable, C., and L. Tauxe, Towards absolute calibration of sedimentary paleointensity records, *Earth Planet. Sci. Lett.*, *143*, 269–274, 1996.

Constable, C. G., L. Tauxe, and R. L. Parker, Analysis of 11 Myr of geomagnetic intensity variation, *Jour. Geophys. Res.*, *103*, 17,735–17,748, 1998.

Cottrell, R. D., and J. Tarduno, In search of high-fidelity geomagnetic paleointensities: A comparison of single plagioclase cyrstals and whole rock Thellier-Thellier analyses, *J. Geophys. Res*, *105*, 23,579–23,594, 2000.

Cox, A. V., Lengths of geomagnetic polarity intervals, *Jour. Geophys. Res.*, *73*, 3247–3260, 1968.

Embley, R., J. Chadwick, W.W., I. Jonasson, D. Butterfield, and E. Baker, Initial results of the rapid response to the 1993 CoAxial event: Relationships between hydrothermal and volcanic processes, *Geophys. Res. Lett.*, *22*, 143–146, 1995.

Embley, R., J. Chadwick, W.W., D. Clague, and D. Stakes, 1998 eruption of axial volcano: multibeam anomalies and sea-floor observations, *Geophys. Res. Lett.*, *26*, 3425–3428, 1999.

Glatzmaier, G. A., R. S. Coe, L. Hongre, and P. H. Roberts, The role of the Earth's mantle in controlling the frequency of geomagnetic reversals, *Nature*, *401*, 885–890, 1999.

Goguitchaichvili, A., L. Alva-Valdivia, J. Rosas-Elguera, J. Urrutia-Fucugauchi, J. A. Gonzalez, J. Morales, and J. Sole, An integrated paleomagnetic study of Rio Grande de Santiago volcanic succession

(trans-Mexican volcanic belt): revisited, *Phys. Earth Planet. Int.*, *130*, 175–194, 2002a.

Goguitchaichvili, A., L. M. Alva-Valdivia, J. Urrutia, J. Morales, and O. F. Lopes, On the reliability of Mesozoic Dipole Low: New absolute paleointensity results from Parana Flood Basalts (Brazil), *Geophys. Res. Lett.*, *29*, doi:10.1029/2002GL015,242, 2002b.

Goguitchaichvili, A., L. M. A. Valdivia, J. R. Elguera, J. U. Fucugauchi, M. A. Cervantes, and J. Morales, Paleosecular variation record of geomagnetic full vector during late Miocene, from the Nayarit area, Mexico, *Phys. Earth Planet. Int.*, *134*, 71–88, 2002c.

Goguitchaichvili, A., J. Morales, E. Canon-Tapia, and R. Negrete, Geomagnetic field strength during late Miocene: First paleointensity results from Baja California, *J. Geophys. Res*, *108*, 10.1029/2002JB002,081, 2003.

Heller, R., R. T. Merrill, and P. L. McFadden, The variation of intensity of earth's magnetic field with time, *Phys. Earth Planet. Int.*, *131*, 237–249, 2002.

Hulot, G., C. Eymin, B. Langlais, M. Mandea, and N. Olsen, Small-scale structure of the geodynamo inferred from Oersted and magsat satellite data, *Nature*, *416*, 620–623, 2002.

Juarez, M., and L. Tauxe, The intensity of the time averaged geomagnetic field: the last 5 m.y., *Earth Planet. Sci. Lett.*, *175*, 169–180, 2000.

Juarez, T., L. Tauxe, J. S. Gee, and T. Pick, The intensity of the Earth's magnetic field over the past 160 million years, *Nature*, *394*, 878–881, 1998.

Kent, D. V., and J. Gee, Magnetic alteration of zero-age oceanic basalt, *Geology*, *24*, 703–706, 1996.

Kirschvink, J. L., The least-squares line and plane and the analysis of paleomagnetic data, *Geophys. Jour. Roy. Astron. Soc.*, *62*, 699–718, 1980.

Larson, R. L., and P. Olson, Mantle plumes control magnetic reversal frequency, *Earth Planet. Sci. Lett.*, *107*, 437–447, 1991.

Loper, D. E., and K. McCartney, Mantle plumes and the periodicity of magnetic field reversals, *Geophys. Res. Lett.*, *13*, 1525–1528, 1986.

Mukasa, S., and J. Ludden, A Campanian-Turonian U-Pb zircon age for plagiogranites from the Troodos ophiolite, *Geology*, *15*, 825–828, 1987.

Perrin, M., E. Schnepp, and V. Shcherbakov, Paleointensity database updated, *EOS, Trans. AGU*, *79*, 198, 1998.

Pick, T., and L. Tauxe, Holocene paleointensities: Thellier experiments on submarine basaltic glass from the East Pacific Rise, *Jour. Geophys. Res.*, *98*, 17,949–17,964, 1993a.

Pick, T., and L. Tauxe, Geomagnetic paleointensities during the Cretaceous normal superchron measured using submarine basaltic glass, *Nature*, *366*, 238–242, 1993b.

Pick, T., and L. Tauxe, Characteristics of magnetite in submarine basaltic glass, *Geophys. J. Int.*, *119*, 116–128, 1994.

Prévot, M., E. A. Mankinen, R. S. Coe, and C. S. Grommé, The Steens Mountain (Oregon) geomagnetic polarity transition 2. Field intensity variations and discussion of reversal models, *J. Geophys. Res*, *90*, 10,417–10,448, 1985.

Rautenschlein, M., G. Jenner, J. Hertogen, A. Hofmann, J. Kerrich, H. Schmincke, and W. White, Isotopic and trace element composition of volcanic glass from the Akaki Canyon, Cyprus: Implications for the origin of the Troodos ophiolite, *Earth Planet. Sci. Lett.*, *75*, 369–383, 1985.

Riisager, J., M. Perrin, P. Riisager, and D. Vandamme, Palaeomagnetic results and palaeointensity of Late Cretaceous Madagascan basalt, *J. Afr. Earth Sci.*, *32*, 503–518, 2001.

Riisager, P., and J. Riisager, Detecting multidomain magnetic grains in Thellier palaeointensity experiments, *Phys. Earth Planet. Inter.*, *125*, 111–117, 2001.

Robinson, P., W. Melson, and H. Schmincke, Volcanic glass compositions of the Troodos ophiolite, Cyprus, *Geology*, *11*, 400–404, 1983.

Selkin, P., and L. Tauxe, Long-term variations in paleointensity, *Phil. Trans. Roy. Soc. Lond.*, *358*, 1065–1088, 2000.

Selkin, P., J. Gee, L. Tauxe, W. Meurer, and A. Newell, The effect of remanence anisotropy on paleointensity estimates: A case study from the Archean Stillwater complex, *Earth Planet. Sci. Lett.*, *182*, 403–416, 2000.

Shi, R. P., R. X. Zhu, Y. X. Pan, G. H. Shi, and K. A. Hoffman, Paleointensity study of Early Miocene lavas from Pingzhuang, Inner Mongolia, China, *Geophys. Res. Lett.*, *29*, doi:10.1029/2002GL015,990, 2002.

Smirnov, A. V., and J. A. Tarduno, Magnetic hysteresis monitoring of Cretaceous submarine basaltic glass during Thellier paleointensity experiments: evidence for alteration and attendant low field bias, *Earth Planet. Sci. Lett.*, *206*, 571–585, 2003.

Stacey, F. D., and S. K. Banerjee, *The Physical Principles of Rock Magnetism*, vol. 5 of *Developments in Solid Earth Geophysics*, Elsevier Sci. Publ. Co., 1974.

Tanaka, H., and M. Kono, Paleointensities from a Cretaceous basalt platform in Inner Mongolia, northeastern China, *Phys. Earth Planet. Int.*, *133*, 147–157, 2002.

Tanaka, H., M. Kono, and H. Uchimura, Some global features of paleointensity in geological time, *Geophys. J. Int.*, *120*, 97–102, 1995.

Tarduno, J., R. Cottrell, and A. Smirnov, High geomagnetic intensity during the mid-Cretaceous from Thellier analyses of single plagioclase crystals, *Science*, *291*, 1779–1782, 2001.

Tarduno, J. A., R. D. Cottrell, and A. V. Smirnov, The Cretaceous superchron geodynamo: Observations near the tangent cylinder, *Proc. Natl. Acad. Sci. U. S. A.*, *99*, 14,020–14,025, 2002.

Tauxe, L., and P. Hartl, 11 million years of Oligocene geomagnetic field behaviour, *Geophys. Jour. Int.*, *128*, 217–229, 1997.

Tauxe, L., and D. V. Kent, A Simplified Statistical Model for the Geomagnetic Field and the Detection of Shallow Bias in Paleomagnetic Inclinations: Was the Ancient Magnetic Field Dipolar?, in press.

Tauxe, L., T. A. T. Mullender, and T. Pick, Potbellies, wasp-waists, and superparamagnetism in magnetic hysteresis, *Jour. Geophys. Res.*, *101*, 571–583, 1996.

Tauxe, L., A. Genevey, Y. Yu, H. Ron, and A. Holtezer, A new paleointensity method and application to Israeli copper mining slag deposits, in prep.

Thellier, E., and O. Thellier, Sur l'intensité du champ magnétique terrestre dans le passé historique et géologique, *Ann. Geophys.*, *15*, 285–378, 1959.

Xu, W. X., D. R. Peacor, W. A. Dollase, R. VanDerVoo, and R. Beaubouef, Transformation of titanomagnetite to titanomaghemite: A slow, two-step, oxidation-ordering process in MORB, *Amer. Mineral.*, *82*, 1101–1110, 1997a.

Xu, W. X., R. VanderVoo, D. R. Peacor, and R. T. Beaubouef, Alteration and dissolution of fine-grained magnetite and its effects on magnetization of the ocean floor, *Earth Planet Sci Lett*, *151*, 279–288, 1997b.

Yu, Y., L. Tauxe, and A. Genevey, Towards an optimal geomagnetic field intensity determination technique, in review.

Zhou, W., R. Van der Voo, and D. Peacor, Single-domain and superparamagnetic titanomagneitte with variable Ti content in young ocean floor basalts: no evidence for rapid alteration, *Earth Planet. Sci. Lett.*, *150*, 353–362, 1997.

Zhou, W. M., D. R. Peacor, R. Van der Voo, and J. F. Mansfield, Determination of lattice parameter, oxidation state, and composition of individual titanomagnetite/titanomaghemite grains by transmission electron microscopy, *J. Geophys. Res.*, *104*, 17,689–17,702, 1999a.

Zhou, W. M., R. Van der Voo, and D. R. Peacor, Preservation of pristine titanomagnetite in older ocean-floor basalts and its significance for paleointensity studies, *Geology*, *27*, 1043–1046, 1999b.

L. Tauxe, Scripps Institution of Oceanography, La Jolla, CA 92093-0220, USA. (e-mail:ltauxe@ucsd.edu)

H. Staudigel, Scripps Institution of Oceanography, La Jolla, CA 92093-0225, USA. (e-mail:hstaudigel@ucsd.edu)

This preprint was prepared with AGU's LaTeX macros v4, with the extension package 'AGU^{++}' by P. W. Daly, version 1.6b from 1999/08/19.

Table 1. Site means using specimens with Grade "A" data (see text).

Site	Lat. (°N)	Long. (°E)	B (μT)	N	σ (μT)	$100(\sigma/B)$	VADM (ZAm^2)	σ_{VADM}
tg001	34.9957	33.2448	22.9	3	1.2	5.2	50.8	2.66
tg002	34.9954	33.2443	22.7	3	2.2	9.7	50.4	4.88
tg004	34.9952	33.2443	26.7	3	3.1	11.7	59.2	6.88
tg006	34.9902	33.2338	13.0	3	2.8	21.4	28.8	6.21
tg008	34.9902	33.2338	18.2	3	3.6	19.7	40.4	7.99
tg009	34.9903	33.2327	19.2	5	4.0	21.0	42.6	8.88
tg010	34.9903	33.2327	15.0	2	1.1	7.5	33.3	2.44
tg011	34.9947	33.2315	13.2	4	3.3	24.9	29.3	7.32
tg015	34.99669	33.23241	24.7	2	1.3	5.2	54.8	2.88
tg019	34.9952	33.2364	8.1	2	1.8	21.7	17.9	3.99
tg020	34.9945	33.2366	39.1	5	3.3	8.5	86.8	7.32
tg021	35.01213	33.154	15.8	5	2.1	13.2	35.0	4.66
tg022	35.01246	33.15416	41.2	4	3.8	9.2	91.4	8.43
tg026	35.0261	33.16338	53.6	6	5.3	9.9	119.	11.7
tg027	35.0261	33.16338	26.5	2	5.0	18.9	58.8	11.1
tg030	35.03768	33.17953	32.6	6	2.3	7.2	72.3	5.10
tg031	35.03766	33.17958	36.3	6	4.9	13.6	80.6	10.8
tg032	35.03708	33.17631	16.1	3	3.3	20.3	35.7	7.32
tg034	35.03134	33.17394	22.7	3	4.7	20.7	50.4	10.4
tg035	35.03146	33.17374	32.7	4	4.4	13.6	72.6	9.77
tg036	35.031	33.17295	28.0	4	3.9	13.8	62.1	8.66
tg037	35.02985	33.17218	39.7	3	0.4	1.0	88.1	0.88
tg038	35.02988	33.17198	77.2	6	4.0	5.2	171.	8.88
tg040	35.02803	33.16597	29.5	8	3.2	10.9	65.5	7.10
tg049	35.00177	33.23631	58.4	2	0.3	0.5	129.	0.66
tg051	35.00141	33.23408	62.1	5	4.6	7.4	137.	10.2
tg052	35.00032	33.2264	51.6	6	6.1	11.8	114.	13.5
tg053	35.00053	33.22619	31.0	7	5.4	17.6	68.8	11.9
tg054	35.00066	33.22615	43.2	2	4.2	9.6	95.9	9.32
tg056	35.00076	33.22589	26.2	2	4.2	16.2	58.1	9.32
tg057	35.000203	33.22195	26.7	3	4.9	18.3	59.2	10.8
tg062	34.9967	33.24726	32.1	2	1.7	5.3	71.2	3.77
tg063	34.9967	33.24726	27.1	3	1.1	4.2	60.1	2.44
tg065	34.99514	33.2483	24.8	2	1.3	5.4	55.0	2.88
tg068	34.99456	33.24889	22.2	5	4.9	22.3	49.2	10.8
tg070	35.00219	33.23716	71.9	2	0.6	0.9	159.	1.33
tg072	35.00219	33.23716	31.8	3	3.3	10.3	70.6	7.32
tg073	35.00232	33.23707	89.7	3	5.3	5.9	199.	11.7
tg077	34.991	33.23281	38.5	4	4.2	11.0	85.4	9.32

$\bar{B}$ is average paleointensity. N is the number of specimens used in the calculation. σ is the standard deviation of $\bar{B}$. VADM is the conversion of $\bar{B}$ to virtual axial dipole moment using an assumed paleolatitude of 20°.

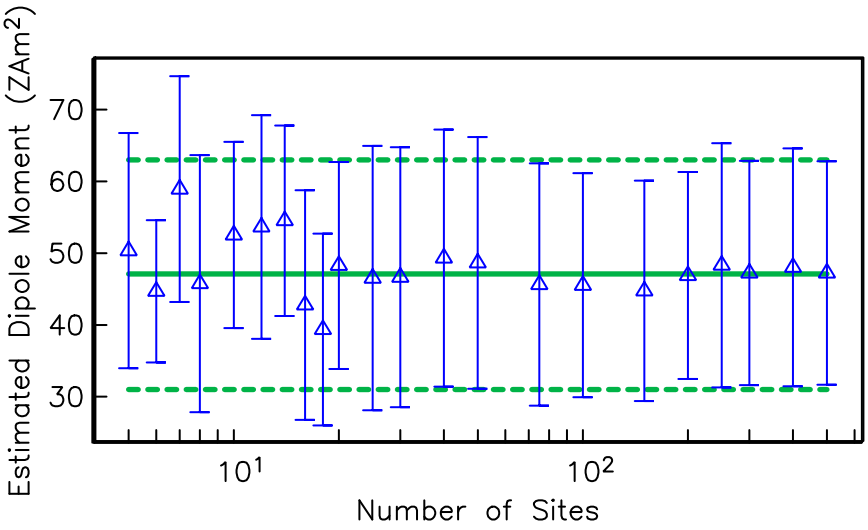

Figure 1. Estimation of average dipole moment from random samples of a statistical field model (TK03.GAD of *Tauxe and Kent* [in press]) as a function of number of sampling sites.

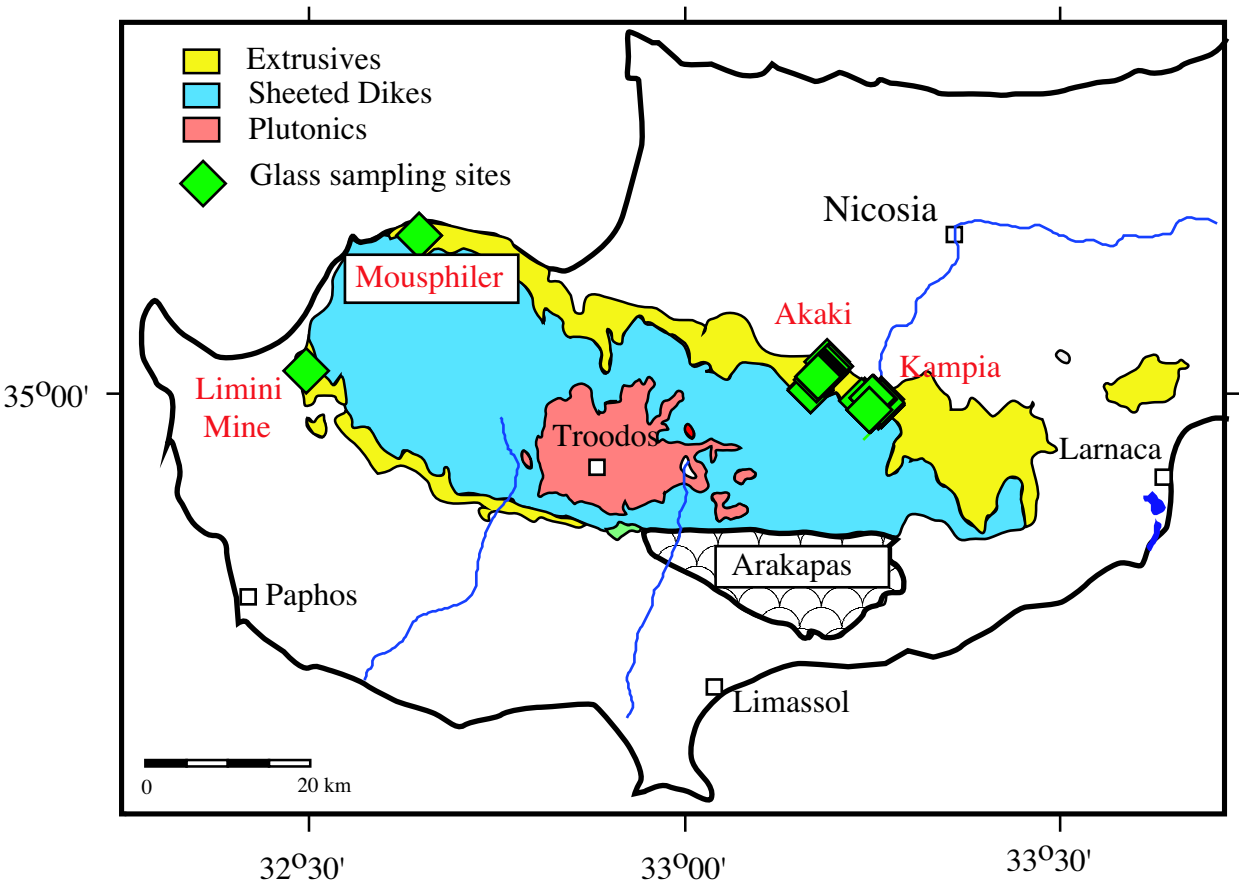

Figure 2. Glass sampling sites from extrusive units in the Troodos Ophiolite. Successful samples came from the Akaki and Kampia regions spanning the entire extrusive crust (except the top 50m) and 10 km of lateral separation.

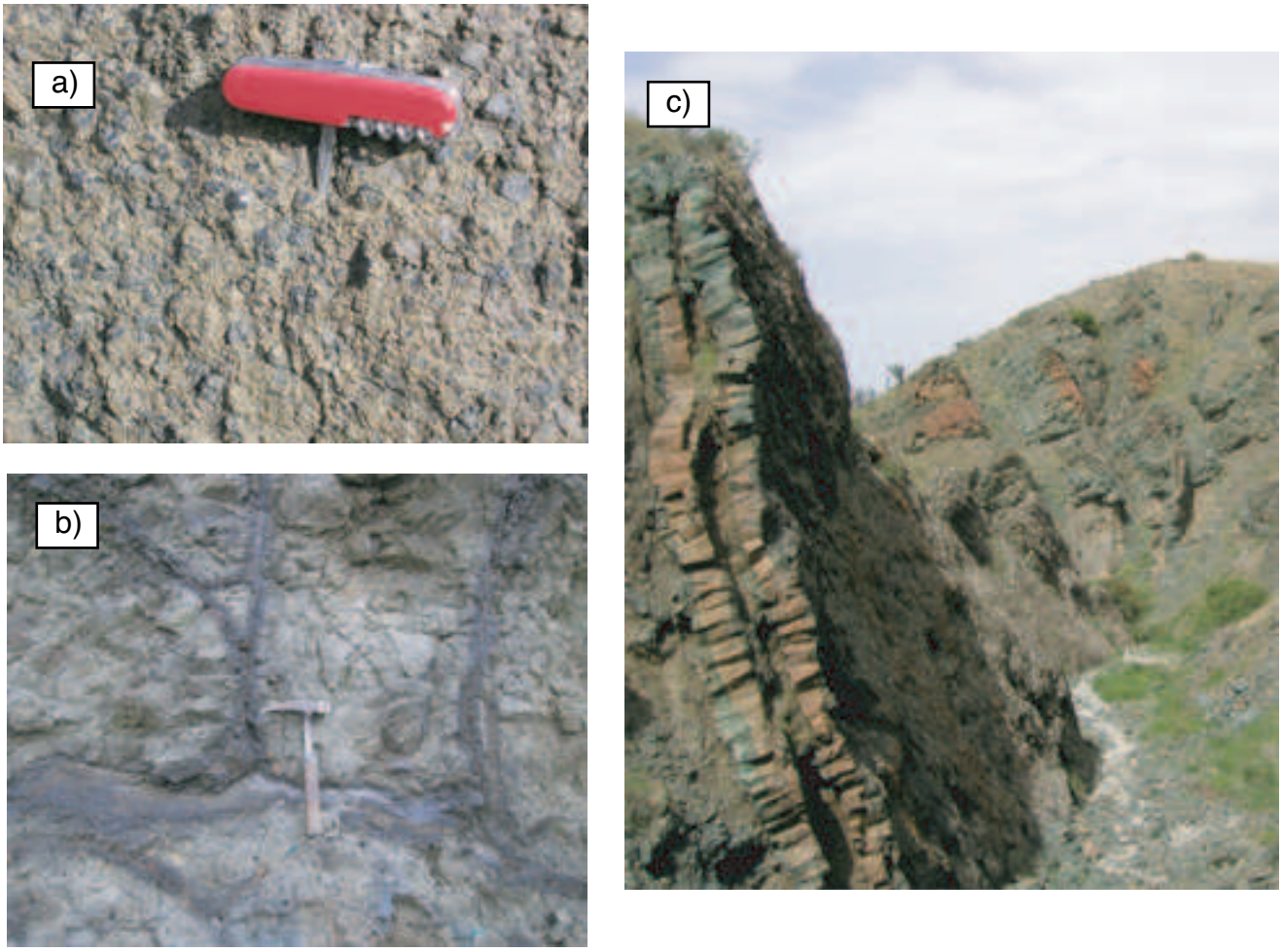

Figure 3. Typical examples of different sampling sites. a) Individual pieces of pillow margin fragments (typically 2 cm in size) were extracted from glassy flows such as this one. b) Pillow margin (darker rim around the pillows often preserved fresh glass. c) Dikes intruding into glassy flows and sheet flows sometimes preserve glassy margins.

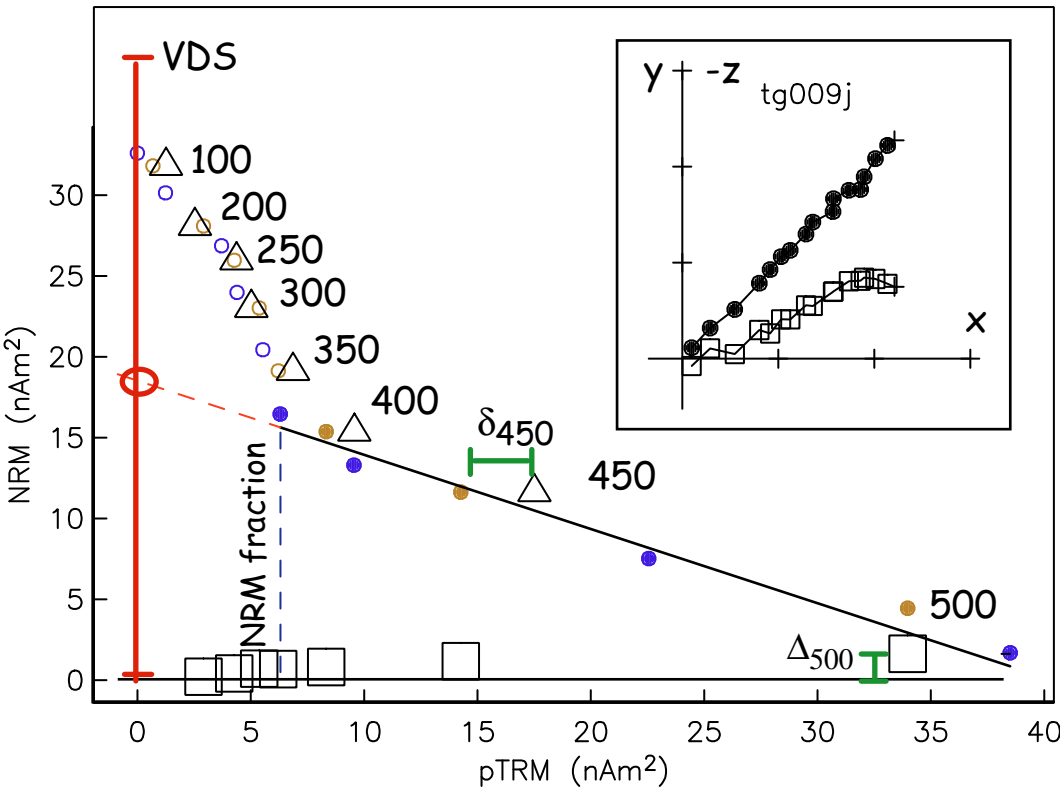

Figure 4. Results of a typical IZZI experiment. Units are magnetic moment in nAm^2. Circles are the pTRM gained at a particular temperature step versus the NRM remaining. Solid symbols are those included in the slope calculation. Blue (darker) symbols are the infield-zerofield steps (IZ, see text) and the brown (lighter) symbols are the zerofield-infield steps (ZI). The triangles are the pTRM checks and the squares are the pTRM tail checks. The difference between the pTRM check and the original measurement is δ_i as shown by the horizontal bar labeled δ_{450}. The difference between the first NRM measurement and the repeated one (the pTRM tail check) is shown by the vertical bar labelled Δ_{500}. The vector difference sum (VDS) is the sum of all the NRM components (tall vertical bar labelled VDS). The NRM fraction is shown by the vertical dashed bar. The normalizer for Coe's f is the intercept of the selected component with the y axis (circled). Our f_{vds} is the NRM fraction normalized by the VDS. The insets are the vector components (x,y,z) of the zero field steps. The solid symbols are (x,y) pairs and the open symbols are (x,z) pairs. The specimens are unoriented with respect to geographic coordinates. The laboratory field was applied along the z-axis in the in-field steps.

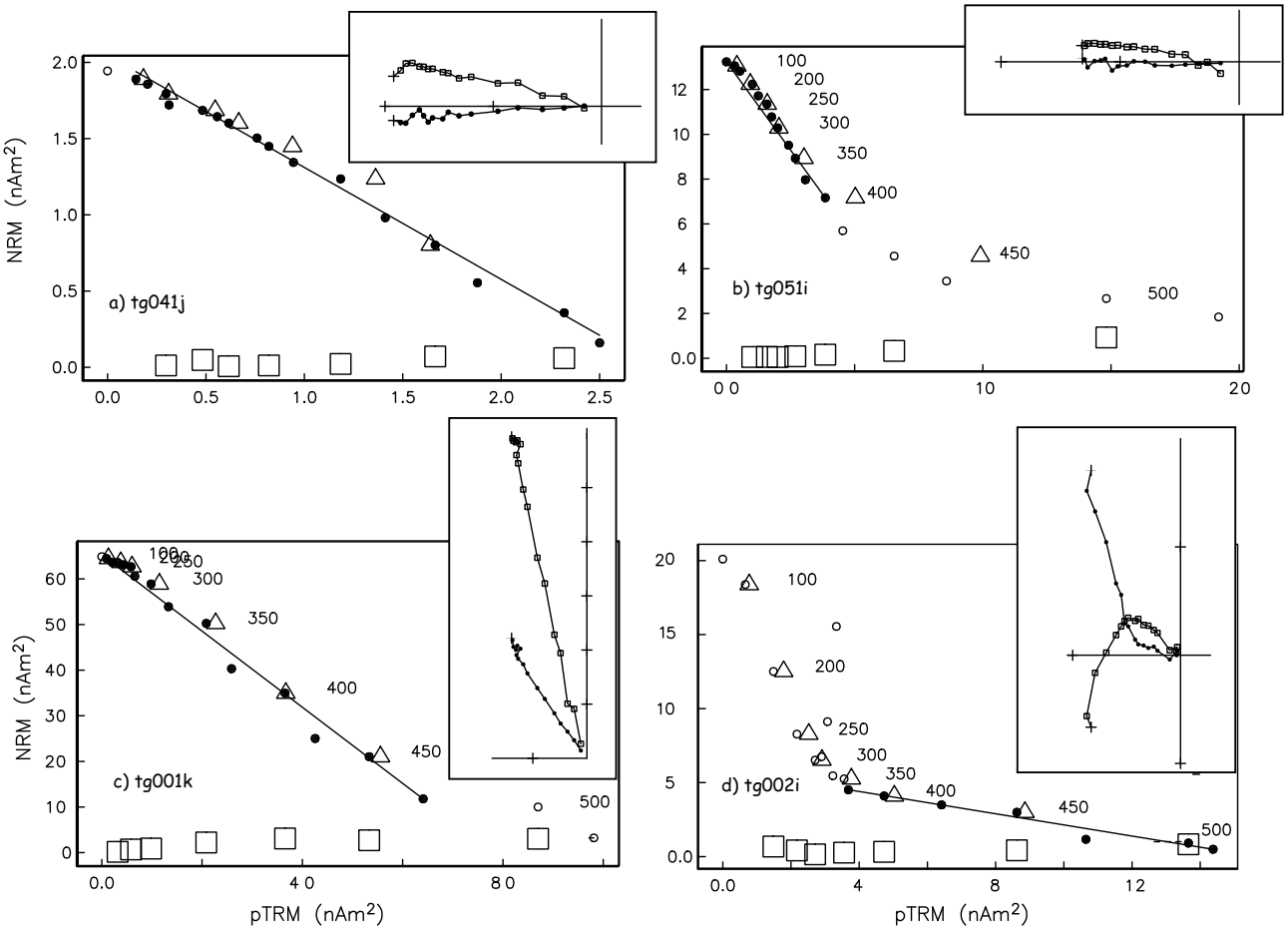

Figure 5. Representative examples of Thellier-Thellier experiments on Troodos Glasses. a) Typical of the best data ($\sim$ 48% of the specimens). b) Exhibits progressively more deviant pTRM checks. c) Exhibits zig-zag behavior with elevated MD% value. d) Has a small f_{vds} and shows directional dependence of zig-zag behavior.

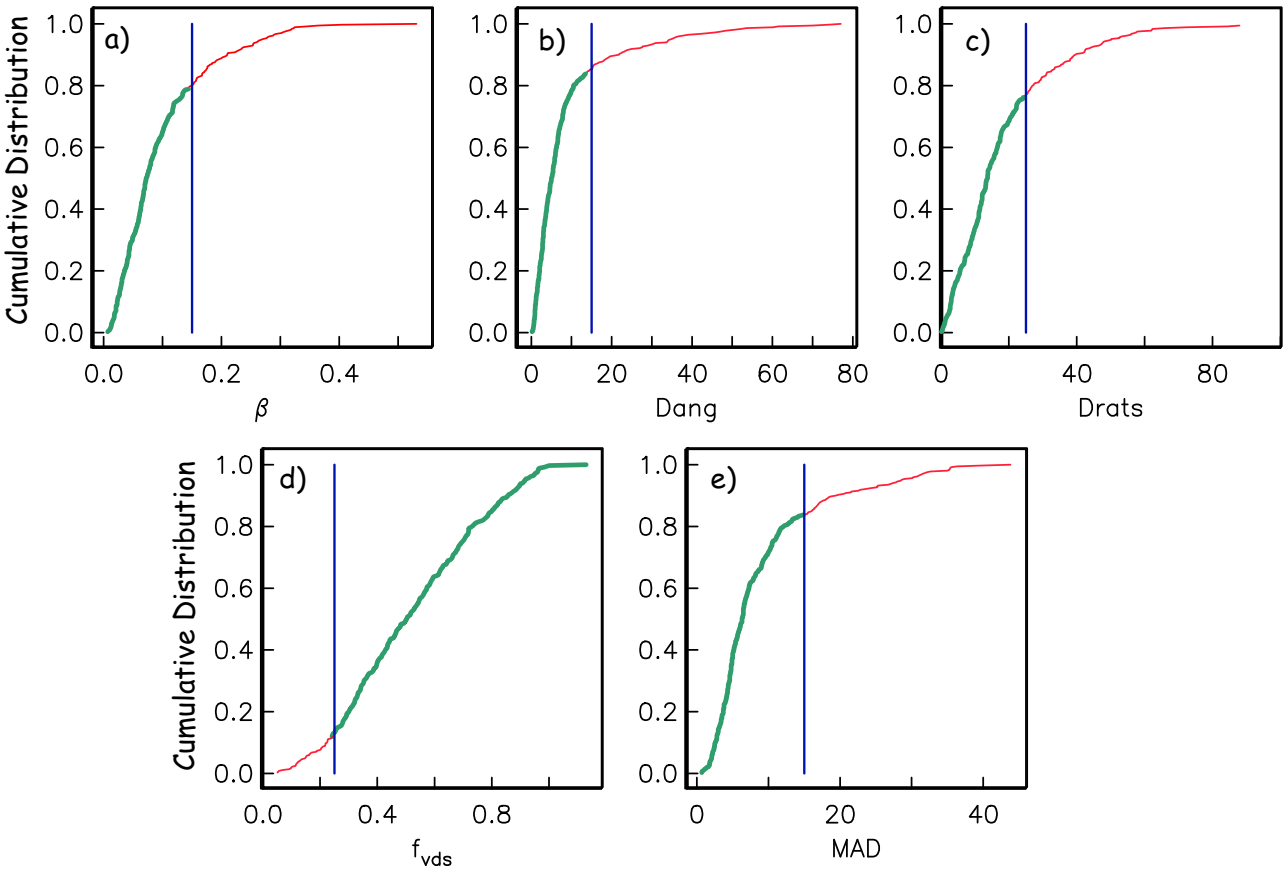

Figure 6. Cumulative distributions of parameters derived from the paleointensity experiments (see text). The vertical lines are the cutoff values used in this paper. The thin (thick) line are values excluded (included) in this study.

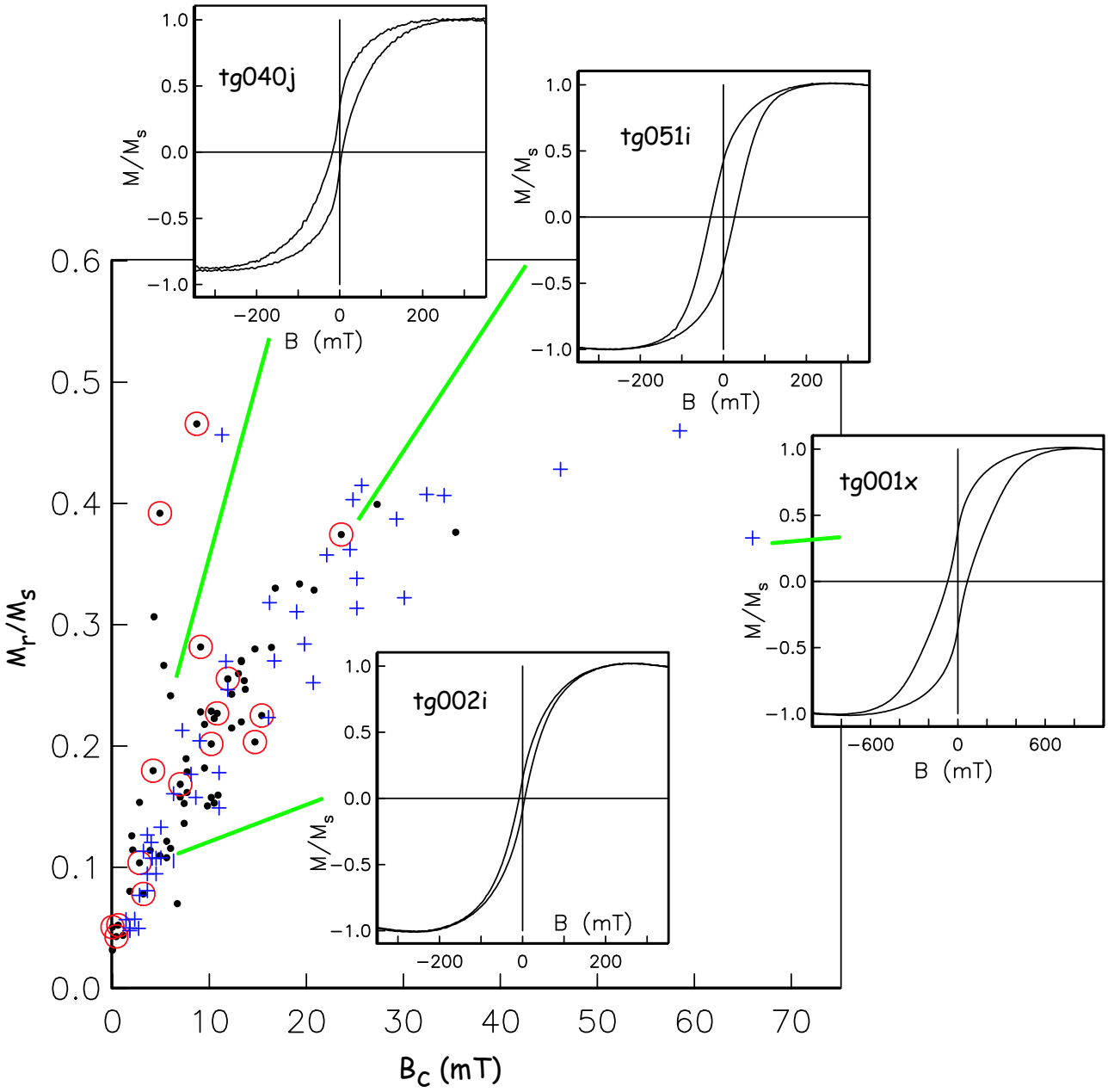

Figure 7. Hysteresis data from representative specimens of Troodos glass. Solid symbols are the specimens measured after completion of the IZZI experiment. Specimens failing the Drat test are circled. Plus signs are unheated sister specimens from the same sites as the solid symbols. Also shown are a few representative hysteresis loops. The behavior of these specimens during the IZZI experiment (except for tg001x which is an unheated sister specimen) is shown in Figure 5.

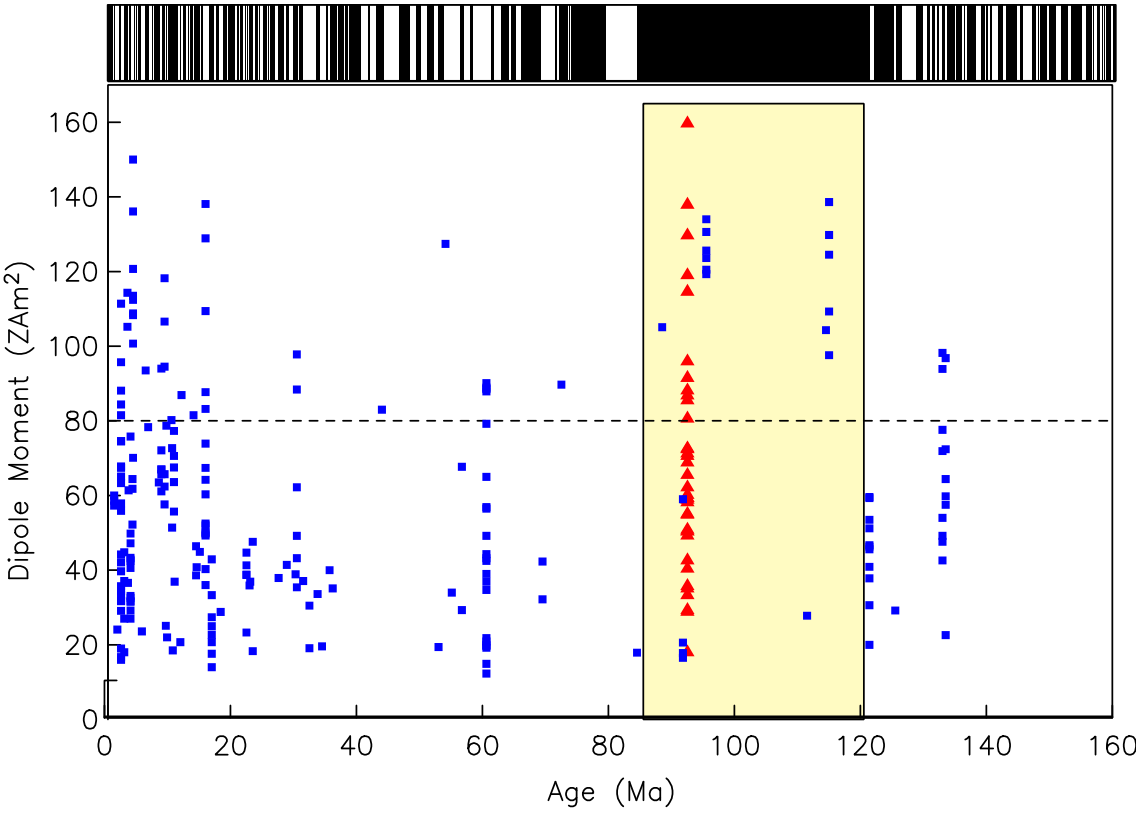

Figure 8. Summary of paleointensity data from this paper and from published sources. All data are from individual cooling units. All paleointensities were converted to VADM using paleolatitudes from a globally consistent set of rotation parameters. Squares: Compilation of published data meeting minimum criteria (see text). Triangles: Data from the Troodos glasses (this paper).

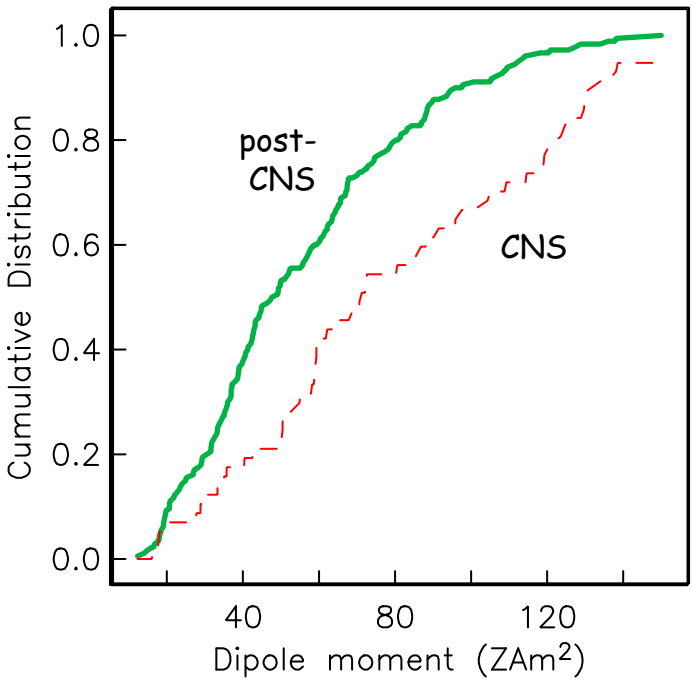

Figure 9. Cumulative distributions of post-CNS data (heavy solid line) and CNS data (thin dotted line). The two distributions are different at above the 99% level of confidence.

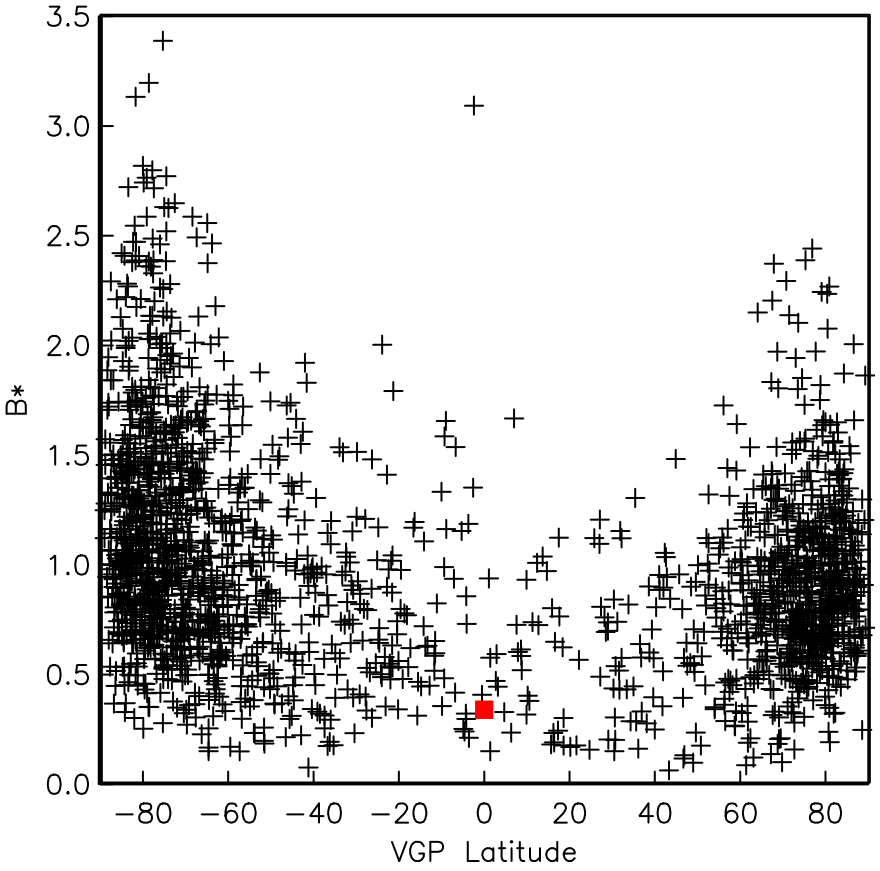

Figure 10. VGP latitude versus relative paleointensity of DSDP Site 522 data of *Tauxe and Hartl* [1997]. The red square is the mean intensity of all transitional specimens as identified in the magnetic stratigraphy.

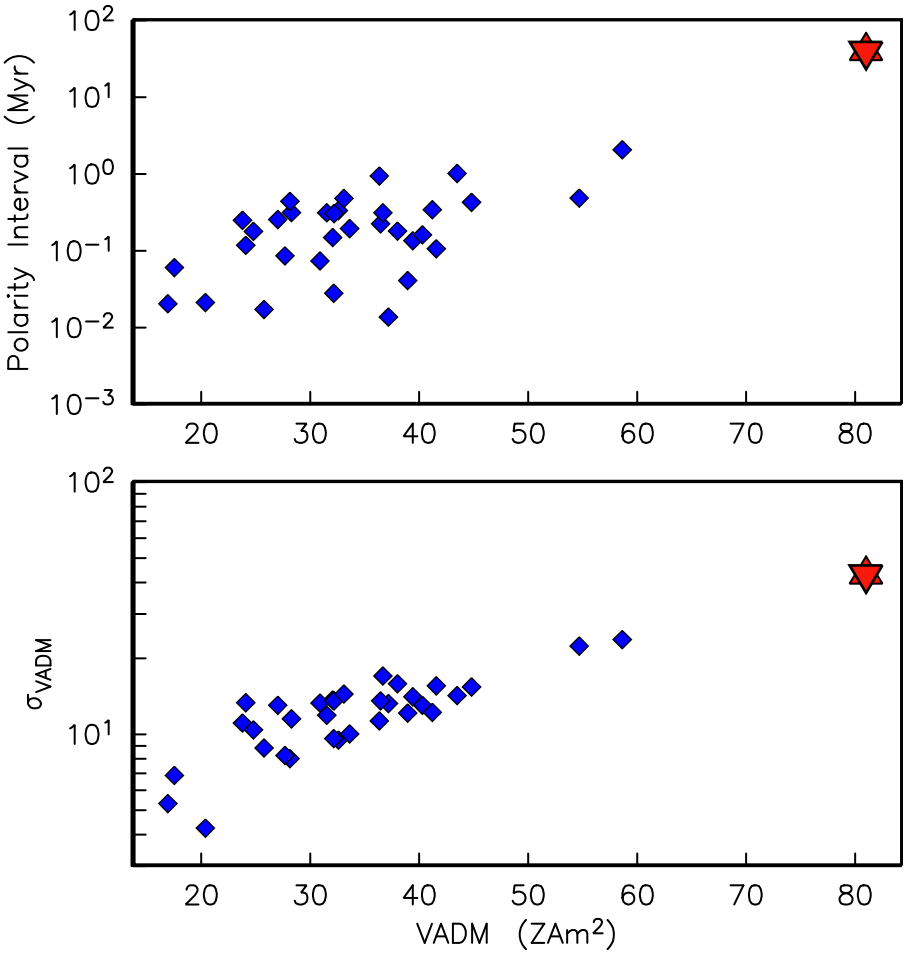

Figure 11. Diamonds are calibrated VADMs from DSDP Site 522 and stars are from the CNS data compiled here. a) VADM versus polarity interval length. b) Standard deviation versus VADM. Figure modified from *Constable et al.* [1998].